Research Article Vol. 60, No. 10 / 1 April 2021 / Applied Optics 2861

applied optics

Geometric layout optimization of a large aperture thin elliptical mirror's axial and lateral support

Peng Guo,[1,2] Jingxu Zhang,[1] Fei Yang,[1,*] Haifei Hu,[1] and Haibo Jiang[1]

[1]Changchun Institute of Optics, Fine Mechanics and Physics, Chinese Academy of Sciences, Changchun 130033, China
[2]University of Chinese Academy of Sciences, Beijing 100049, China
*Corresponding author: yangf@ciomp.ac.cn

Received 7 December 2020; revised 9 March 2021; accepted 9 March 2021; posted 11 March 2021 (Doc. ID 405638); published 26 March 2021

For passive support of large aperture telescopes, geometric layout optimization of the support structure is one of the most critical tasks because it determines the deformation of the mirror under gravity, which affects the wavefront aberration and image quality of the system. Due to a lack of symmetry, the optimization of an elliptical mirror support can be much more complex compared with circular mirrors. We optimize the geometric layout of axial and lateral support for the tertiary mirror of the Thirty Meter Telescope (TMT). Based on a theoretical analysis of the whiffletree principle, a parametric model of axial support is established based on the multi-point constraint equation. The mirror deformation SlopeRMS of the tertiary mirror under vertical gravity is used as the optimization target of the support points. The axial support point position is optimized by means of a simulated annealing algorithm and a mirror-deformed post-processing script written in Python. The TMT tertiary mirror lateral support also uses the whiffletree structure, and its in-plane layout affects the system's resonant modal frequency and the maximum load at each point. According to the dynamic equation and the static principle, the lateral support optimization model is established. The first-order resonant frequency and maximum load of the support point are the objective function. Through optimization of the axial and lateral support, the overall mirror distortion of the system is improved.

https://doi.org/10.1364/AO.405638

1. INTRODUCTION

The optical telescope is a sophisticated device with a high image quality requirement. To accomplish this, its mirror surface deformation due to gravity or thermal distortion has to be decreased to an acceptable value. The mirror must be isolated from extra stress by kinematically constraining its six degrees of freedom (DOFs) in space, since over-constraint will bring in additional stress and strain on the mirror. The mirror support system design must follow the kinematical principle. Typically, the support system consists of axial support and lateral support, and each support constrains four DOFs [1].

When the mirror's optical axis is vertical, its weight is all taken by axial support, and the gravity deflection is strongly correlated with the support points' locations, especially for axial support. Hence, the axial support points' layout must be optimized to minimize the mirror surface deformation under gravity. In 1945, Hindle proposed a nine-point and an 18-point axial support for a circular mirror with a central hole [2]. The support points lie in two rings with optimized radii around the center of the mirror. Furthermore, in 1982, Nelson developed theoretical optimum axial support point distribution for a circular mirror based on the thin plate theory [3]. Based on his work, the root mean square (RMS) of the mirror surface error can be evaluated by Eq. (1):

$$\delta = \lambda(q/F)(A/N)^2, \tag{1}$$

$$F = \frac{Et^3}{12(1-\mu)}, \tag{2}$$

where δ denotes the mirror surface RMS; q denotes the average force acting on the plate; A denotes the plate's area; N denotes the count of support points; F denotes the flexibility of the plate, which can be calculated by Eq. (2); E denotes the elastic modulus of the mirror's material; t denotes the mirror's thickness; and μ denotes the material's Poisson ratio.

Nelson also studied the optimal geometry layout of support points for circular plate. However, this analytical work applies only to a circular thin flat mirror. For an irregularly shaped mirror, its deflection can be precisely predicted with the aid of finite element analysis (FEA). For instance, the primary mirror of TMT utilizes FEA to predict the mirror surface and optimize the support points [3,4].

Lateral support takes the mirror weight perpendicular to the optical axis. A widely used passive lateral support is push–pull

support accomplished by implementing astatic levels around the mirror. Schwesinger studied the optimization of push–pull support and presented the optimal support force distribution [5]. This kind of support had been proved efficient and reliable in the Very Large Telescope. The astatic level system can automatically balance the weight component of the mirror when the altitude angle changes.

The Thirty Meter Telescope (TMT) is a next-generation ground-based telescope under construction. Its tertiary mirror, also called the Giant Steerable Science Mirror (GSSM), is a folded flat elliptical mirror with dimensions of 3620 mm × 2550 mm × 100 mm [6]. The support system requires it to be a passive kinematical system. GSSM's giant size and mass pose a challenge for the design of the mirror's support system to meet the requirement of the mirror surface, resonant frequency, and load capacity. This paper describes methods used in the geometric optimization of GSSM's axial and lateral support. Section 2 introduces the structure overview of GSSM and especially the support structure. Section 3 discusses the optimization objective function selection for axial and lateral support. Section 4 describes the modeling method of axial support and its optimization. Section 5 presents the optimization of lateral support based on its maximum shear load on support and the first-order resonant frequency. Section 6 concludes the optimization results.

2. GSSM OVERVIEW

As shown in Fig. 1, GSSM locates above the center hole of the primary mirror and relays the light from the second mirror to the science instruments mounted on the Nasmyth platform. It rotates around the elevation axis together with the primary mirror during observation. The mechanical structure of GSSM consists of an M3 cell assembly (M3CA) and M3 pointing assembly (M3PA). M3CA provides support for the mirror under gravity to maintain the mirror surface distortion at an acceptable value. M3PA is the GSSM mount with two perpendicular axes, tilt and rotation, which allow the mirror rotate and tilt around the axes during telescope observation or switching different instruments.

In 2008, Myung Cho studied and proposed a concept of active support consisting of 84 actuators with excellent performance of correcting the mirror's aberration [7]. However, considering that an active optics M3 will increase the system's cost and complexity, TMT decided to use passive support, which is more reliable and simpler [1]. The support structure of GSSM is shown in Fig. 1. The axial support is an 18-point whiffletree, which is just like Hindle's support concept, except the mirror is elliptical, not circular. The basic kinematical concept of lateral support is three tangent rods around the mirror. Mirror weight is over 1.8 ton and three support points generate unacceptable stress on the mirror and support structure. Hence, the lateral support adopts a 12-point whiffletree system to

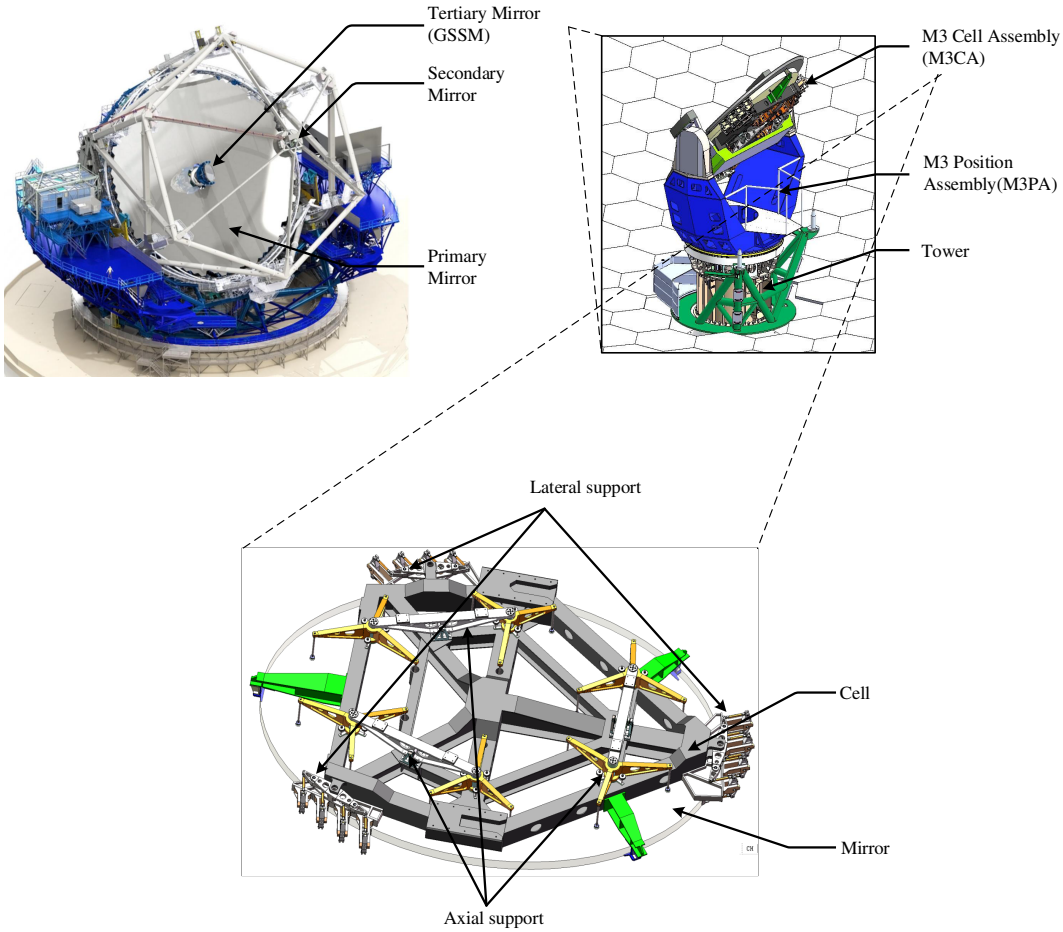

Fig. 1. Plot of support structure of GSSM.

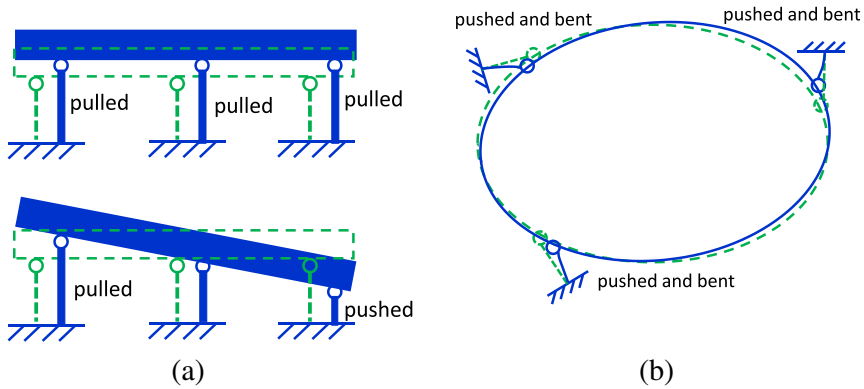

Fig. 2. (a) Axial support modes and (b) lateral support mode.

increase support points, which is still equivalent to three tangent supports in kinematics. The support points are all co-plane with the middle plane of the mirror where the center of gravity (CG) lies.

3. SELECTION OF OPTIMIZATION OBJECTIVE FUNCTION

Axial support and lateral support have different mechanical characteristics, so the corresponding objective function is selected accordingly. Compared with lateral support, the axial support structure is much stiffer. This is because the support rod is very stiff in the axial direction but flexible in a bent or transverse direction. The axial modes of the mirror are piston and tip/tilt. Their stiffness is very high, because all the axial rods are pushed/pulled under these modes, as shown in Fig. 2(a). So these modes' stiffness comes from the rods' axial stiffness.

Lateral support can be treated as a mass support by three springs in-plane. But modes of lateral support are mirror torsion or translation in-plane. As shown in Fig. 2(b), these modes cause the support rods to be not only pushed/pulled, but also bent. Hence, the lateral mode's stiffness is much less than that of axial modes, and the first-order mode of the whole system is one of the lateral modes. So we choose the first-order resonant frequency as an objective function for lateral support optimization.

As for the mirror surface deformation, the mirror is a thin plate. Hence, it is very flexible along the normal direction of the mirror surface, but very stiff along the transverse direction. So axial deformation is much larger than lateral, as shown in Fig. 3(a). The mirror surface axial support is very sensitive to support points' locations, so the support points' locations must be optimized based on the mirror surface.

On the contrary, as long as the lateral support points are in the middle plane of the mirror, the lateral deformation is mainly in-plane, as shown in Fig. 3(b). The mirror surface deformation will be just some local small bumps, which is much smaller than axial support deformation. So we choose mirror surface deformation as the objective function for axial support optimization.

Also, the stress on the mirror is a critical requirement, and lateral support stress is higher than axial support stress due to fewer support points and the bending effect. Therefore, lateral support optimization also considers the stress on the mirror. This will be presented and further discussed in Section 5.A.

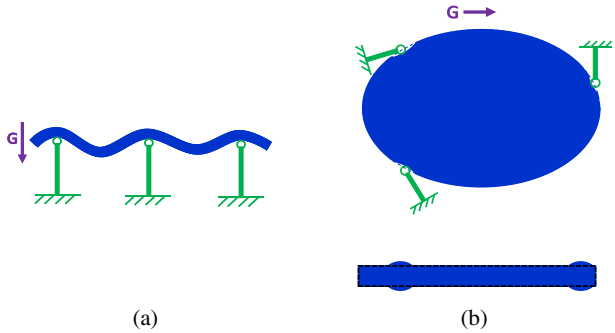

Fig. 3. (a) Mirror surface deformation of axial support and (b) mirror surface deformation of lateral support.

4. OPTIMIZATION OF AXIAL SUPPORT

A. Whiffletree Equivalent Multi-Point Constraint

The layout of the 18-point axial whiffletree system is as shown in Fig. 4. The whiffletree system consists of six tripods and three rockers. The triangle pivot is a universal joint with two rotation DOFs, and the rocker pivot has one rotation DOF. The 18 support points and pivots are symmetric about x and y axes. Hence, the support system can be described by independent coordinates of support points and pivots in the first quadrant.

The axial support is built as a parametric finite element model (FEM) by the Ansys Parametric Design Language (APDL). The tripod's virtual movement can be decomposed as two rotations around the pivot [8]. The support point locations after rotation can be calculated by multiplying its original location with two rotational transformation matrices:

$$R_{\mathrm{rot}_x} = \begin{bmatrix} 1 & & \\ & \cos(\mathrm{rot}_x) & -\sin(\mathrm{rot}_x) \\ & \sin(\mathrm{rot}_x) & \cos(\mathrm{rot}_x) \end{bmatrix}, \tag{3}$$

$$R_{\mathrm{rot}_y} = \begin{bmatrix} \cos(\mathrm{rot}_y) & & \sin(\mathrm{rot}_y) \\ & 1 & \\ -\sin(\mathrm{rot}_y) & & \cos(\mathrm{rot}_y) \end{bmatrix}, \tag{4}$$

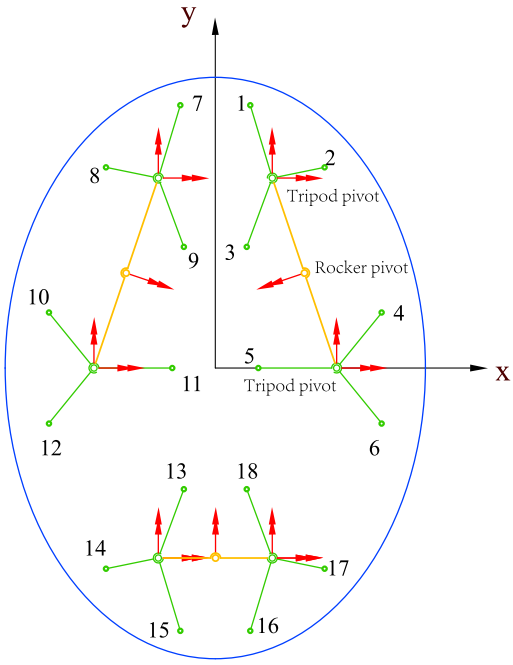

Fig. 4. Axial support points layout.

$$\begin{bmatrix} x'_i \\ y'_i \\ z'_i \end{bmatrix} = R_{\mathrm{rot}_x} R_{\mathrm{rot}_y} \begin{bmatrix} x_i \\ y_i \\ z_i \end{bmatrix}, \tag{5}$$

where x_i, y_i and z_i are original location coordinates of support point i, and x'_i, y'_i and z'_i are the coordinates after rotation. We use $U_{x,i}$, $U_{y,i}$ and $U_{z,i}$ to represent the deformation of support point i in three directions. Then the displacement of the support point can be solved as

$$U_{x,i} = x'_i - x_i = x_i(\cos(\mathrm{rot}_y) - 1), \tag{6}$$

$$U_{y,i} = y'_i - y_i = y_i(\cos(\mathrm{rot}_x) - 1) - x_i \sin(\mathrm{rot}_x) \sin(\mathrm{rot}_y), \tag{7}$$

$$U_{z,i} = z'_i - z_i = -y_i \sin(\mathrm{rot}_x) - x_i \cos(\mathrm{rot}_x) \sin(\mathrm{rot}_y), \tag{8}$$

$$i = 1, 2, 3. \tag{9}$$

Under small deformation conditions, these expressions could be substituted with their first-order Taylor expansions as $\sin(x) \approx x$ and $\cos(x) \approx 1 - 2x^2$. After ignoring the high-order small quantities in the expressions, $U_{x,i}$, $U_{y,i}$, and $U_{z,i}$ are

$$U_{x,i} = 0, \tag{10}$$

$$U_{y,i} = 0, \tag{11}$$

$$U_{z,i} = -y_i \mathrm{rot}_x - x_i \mathrm{rot}_y, \tag{12}$$

$$i = 1, 2, 3. \tag{13}$$

So the movements $U_{x,i}$ and $U_{y,i}$ are negligible compared with $U_{z,i}$. After eliminating the two variables rot_x and rot_y, the three equations can be reduced to a linear one that consists of $U_{z,i}$:

$$\sum_i \omega_i U_{z,i} = 0, \quad i = 1, 2, 3. \tag{14}$$

The coefficient ω can be calculated by the points' locations (x_i, y_i) and the pivot's location $(x_{\mathrm{piv}}, y_{\mathrm{piv}})$. When combining the triangle and rocker, we need to combine the equations. The whiffletree system can be simulated by using a multi-point constraint (MPC) to constrain the support points as this equation. Based on the principle of virtual work, the reaction force at each support point F_i meets the following equation:

$$\sum_i F_i U_{z,i} = 0, \quad i = 1, 2, 3. \tag{15}$$

Based on Eq. (2), the force distribution is

$$\frac{F_1}{\omega_1} = \frac{F_2}{\omega_2} = \frac{F_3}{\omega_3}. \tag{16}$$

The coefficient ω determines the constraint force at the support point. This is because ω is relevant to the pivot's location, and changing ω will change the pivot's location. The relation between ω and the pivot's location can be solved by the former equation:

$$\sum_i F_i(x_i - x_0) = 0, \tag{17}$$

$$\sum_i F_i(y_i - y_0) = 0. \tag{18}$$

Solving Eqs. (17) and (18) can obtain the pivot's location as follows:

$$x_0 = \frac{\sum_i F_i x_i}{\sum_i F_i} = \frac{\sum_i \omega_i x_i}{\sum_i \omega_i}, \tag{19}$$

$$y_0 = \frac{\sum_i F_i y_i}{\sum_i F_i} = \frac{\sum_i \omega_i y_i}{\sum_i \omega_i}. \tag{20}$$

Support point 6 and support point 4 are symmetric about the x axis, so ω_6 and $U_{z,6}$ are equal to ω_4 and $U_{z,4}$, respectively. The equivalent equation of the whiffletree can be written as

$$\omega_1 U_{z,1} + \omega_2 U_{z,2} + \omega_3 U_{z,3} = 0, \tag{21}$$

$$\omega_4 U_{z,4} + 2\omega_5 U_{z,5} = 0. \tag{22}$$

Since the rocker's pivot is generally designed at the middle point of the rocker, the two resultant forces of the tripods at the end of the rocker are equal:

$$F_5 + 2F_4 = F_1 + F_2 + F_3. \tag{23}$$

Therefore, the coefficients ω_i meet

$$\omega_5 + 2\omega_4 = \omega_1 + \omega_2 + \omega_3. \tag{24}$$

In these equations, one of the coefficients ω_i is redundant and can be set as one. We choose to take ω_5 as one. Then, based on Eq. (24), ω_4 can be expressed as a combination of ω_1, ω_2, and ω_3. Hence three independent coefficients, ω_1, ω_2, and ω_3, can completely determine the location of the whiffletree's pivot. Thus, the axial whiffletree can be described by nine design variables, which are $x_1, x_2, y_2, x_3, y_3, x_4, y_4, x_5, y_5, \omega_1, \omega_2$, and ω_3.

B. Mirror Surface Evaluation

Optical performance is the driven goal of support optimization. The science metric function of TMT is normalized point source sensitive (PSSn), which is calculated by

$$\mathrm{PSS}_{\mathrm{Normalized}} = \frac{\int_\infty |\mathrm{PSF}_{\mathrm{Err}}(\theta)|^2 \mathrm{d}\theta}{\int_\infty |\mathrm{PSF}_o(\theta)|^2 \mathrm{d}\theta}. \tag{25}$$

In this equation, $\mathrm{PSF}_{\mathrm{Err}}$ denotes the power spectrum function of the mirror with external disturbances such as gravity sag, wind, atmosphere, etc., and PSF_0 denotes the power spectrum function of an ideal system.

PSSn indicates the real system's deviation from a perfect one and reflects the image quality of the telescope system under the influence of various aspects of error. However, PSSn is not suitable for being an objective function, since it is not convenient for calculation. Based on TMT's previous research, mirror surface SlopeRMS, which is RMS of slopes of the mirror surface error, is well correlated to corresponding PSSn, as expressed by

$$\mathrm{PSSn} = 1 - \mathrm{cSlopeRMS}^2. \tag{26}$$

SlopeRMS can be directly computed by

$$\mathrm{SlopeRMS} = \sqrt{\left(\frac{1}{(N-1)(M-1)}\right)\sum_{i=1}^{N-1}\sum_{i=1}^{N-1}\left(\left(\frac{z_{i+1,j} - z_{i,j}}{\mathrm{d}x}\right)\right)}. \tag{27}$$

$z_{i,j}$ denotes the mirror surface sag along z direction, which was extracted from FEM and interpolated to a set of predefined 3.4 mm pitch grid size. When the mirror's axis is vertical pointing, the mirror surface due to gravity is fully dependent on the axial support. We use $\mathrm{SlopeRMS}_{\mathrm{vertical}}$ to represent the mirror surface SlopeRMS under this load condition, and it will be used as the objective function:

$$\Phi = \mathrm{SlopeRMS}_{\mathrm{vertical}}. \tag{28}$$

C. Optimization Procedure

Based on the work above, the optimization model of axial support can be expressed as

Table 1. Optimization Results of Axial Support

Support Design	Initial Value (mm)	Optimized Value (mm)
x_1	357.3	356.815
x_2	297.27	319.495
x_3	773.5	784
x_4	256.99	234.282
x_5	983.96	968.693
y_2	1465.2	1466.32
y_3	1016	986.043
y_4	683.1	648.278
y_5	351.75	319.137
w_1	1	1.0431
w_2	1	1.0198
w_3	1	1.0189
$\mathrm{SlopeRMS}_{\mathrm{vertical}}$	1.046	1.033

$$\min \quad \Phi \qquad \text{s.t.} \quad \begin{cases} 200 < x_1 < 400 \\ 150 < x_2 < 350 \\ 700 < x_3 < 900 \\ 200 < x_4 < 400 \\ 850 < x_5 < 1050 \\ 1350 < y_2 < 1550 \\ 900 < y_3 < 1100 \\ 550 < y_4 < 750 \\ 200 < y_5 < 400 \\ 0.9 < \omega_1 < 1.1 \\ 0.9 < \omega_2 < 1.1 \\ 0.9 < \omega_3 < 1.1 \end{cases}. \tag{29}$$

In this equation, x_1, x_2, x_3, x_4, and x_5 refer to the x coordinates of support points; y_2, y_3, y_4, and y_5 are the y coordinates of support points; and ω_1, ω_2, ω_3 are the weight of support points 1, 2, 3 in the MPC equations.

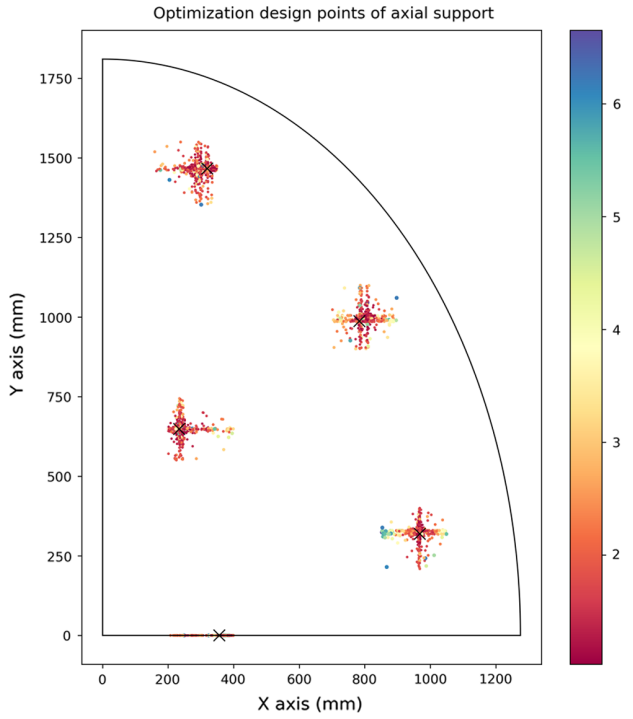

Fig. 5. Distribution of axial support points during optimization.

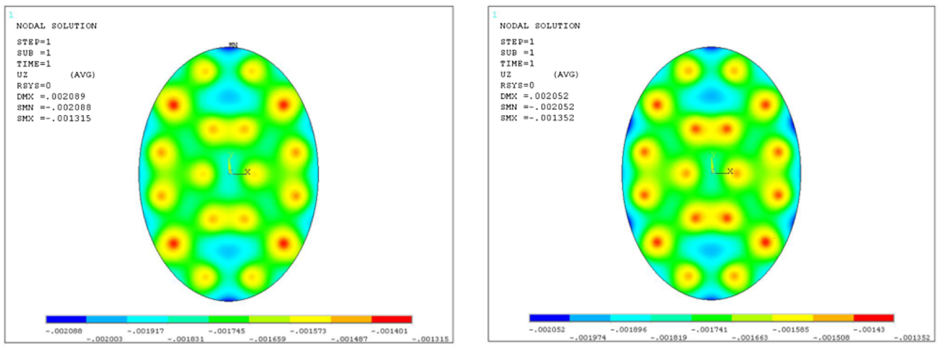

(a) (b)

Fig. 6. (a) Mirror surface figure of initial support points and (b) mirror surface after optimization.

The model involves 12 design variables, so there are many local optimum solutions in the process. Gradient algorithms or direct search algorithms are not suitable, because they are sensitive to an initial solution and hard to jump out of a local valley. Global algorithms such as the genetic algorithm, particle swarm optimization, and adaptive simulated annealing usually perform better for this kind of problem [9]. Finally, the adaptive simulated annealing algorithm was adopted. The initial points are manually optimized support points that have achieved good performance. The optimized results and performances are listed in Table 1. The distributions of all feasible support points are plotted in Fig. 5. The colors of the points indicate the SlopeRMS of the mirror surface under this set of points. The black "x" marks the optimal support position.

Figure 6 shows the mirror surface after optimization. The SlopeRMS under axial support decreased from the initial value of 1.046 μrad to 1.033 μrad.

5. OPTIMIZATION OF LATERAL GEOMETRY

Lateral support supports the gravity components along x and y directions [10]. The lateral support points are all in the CG plane to reduce the mirror surface deformation under gravity, which is very sensitive to the support points' deviation from the CG plane. The whiffletree's direction and location in the CG plane basically do not affect the mirror surface [11]. However, the geometry layout affects the support's load distribution and dynamic performance. As shown in Fig. 7, The lateral support can be treated as a planar mechanism consisting of a concentric mass and three in-plane springs [10]. A spring's location and direction affect the stiffness matrix of the system, which affects the system's resonant frequency and mode shape.

A. Lateral Support Static Formulation

The reaction forces at the support points of the same group of whiffletrees are equal in magnitude and parallel in direction. The resultant force passes through the pivot of the whiffletree in the same direction. The three whiffletrees' resultant forces F_1, F_2, and F_3 are balanced with gravity. When gravity acts in the lateral plane, it can be described by angle β to the x axis. F_1, F_2, and F_3 will change along with gravity vector angle β. The lateral static force equilibrium equations are

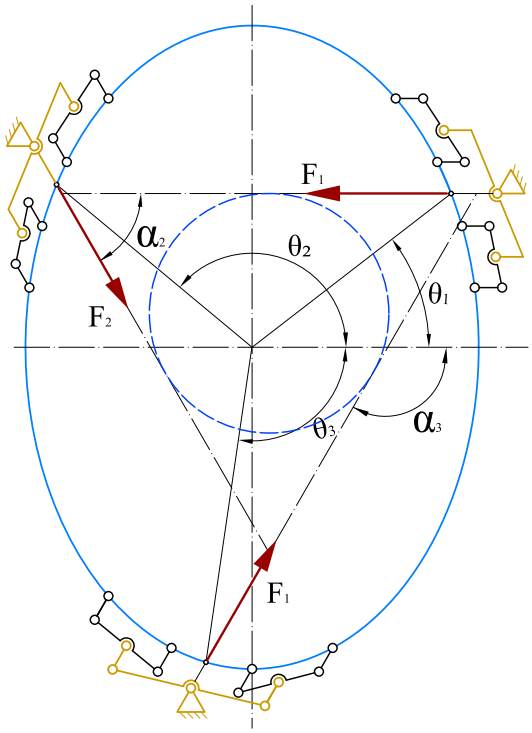

Fig. 7. Lateral support equivalent.

$$F_1 \cos\alpha_1 + F_2 \cos\alpha_2 + F_3 \cos\alpha_3 = G\cos\beta, \tag{30}$$

$$F_1 \sin\alpha_1 + F_2 \sin\alpha_2 + F_3 \sin\alpha_3 = G\sin\beta, \tag{31}$$

$$F_1 d_1 + F_2 d_2 + F_3 d_3 = 0. \tag{32}$$

Solving the equilibrium equation, we get

$$F_1 = \frac{d_3 \sin\beta - \alpha_2 - d_2 \sin\beta - \alpha_3}{d_1 \sin\alpha_2 - \alpha_3 + d_2 \sin\alpha_3 - \alpha_1 + d_3 \sin\alpha_1 - \alpha_2}, \tag{33}$$

$$F_2 = \frac{d_1 \sin\beta - \alpha_3 - d_2 \sin\beta - \alpha_1}{d_1 \sin\alpha_2 - \alpha_3 + d_2 \sin\alpha_3 - \alpha_1 + d_3 \sin\alpha_1 - \alpha_2}, \tag{34}$$

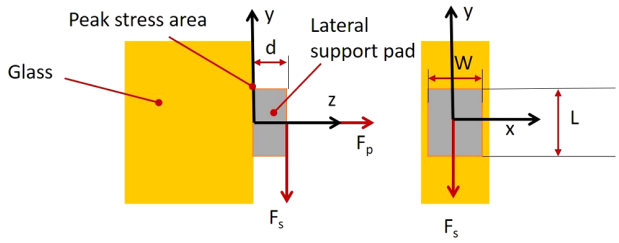

Fig. 8. Stress on the lateral support.

$$F_3 = \frac{d_3 \sin\beta - \alpha_1 - d_2 \sin\beta - \alpha_2}{d_1 \sin\alpha_2 - \alpha_3 + d_2 \sin\alpha_3 - \alpha_1 + d_3 \sin\alpha_1 - \alpha_2}. \tag{35}$$

Based on the trigonometric equations, the maximum force of each lateral support during gravity change can be solved as

$$F_{1,p} = \frac{\sqrt{d_2^2 + d_3^2 - 2d_2 d_3 \cos(\alpha_2 - \alpha_3)}}{d_1 \sin(\alpha_2 - \alpha_3) + d_2 \sin(\alpha_3 - \alpha_1) + d_3 \sin(\alpha_1 - \alpha_2)}, \tag{36}$$

$$F_{2,p} = \frac{\sqrt{d_2^2 + d_3^2 - 2d_2 d_3 \cos(\alpha_2 - \alpha_3)}}{d_1 \sin(\alpha_2 - \alpha_3) + d_2 \sin(\alpha_3 - \alpha_1) + d_3 \sin(\alpha_1 - \alpha_2)}, \tag{37}$$

$$F_{3,p} = \frac{\sqrt{d_2^2 + d_3^2 - 2d_2 d_3 \cos(\alpha_2 - \alpha_3)}}{d_1 \sin(\alpha_2 - \alpha_3) + d_2 \sin(\alpha_3 - \alpha_1) + d_3 \sin(\alpha_1 - \alpha_2)}. \tag{38}$$

The corresponding β of the three maximum forces are

$$\beta_i = 90 - a \cos\left(\frac{d_{i+2}\cos(\alpha_{i+1}) - d_{i+1}\cos(\alpha_{i+2})}{d_{i+1}^2 + d_{i+2}^2 - 2d_{i+1}d_{i+2}\cos(\alpha_{i+1} - \alpha_{i+2})}\right). \tag{39}$$

Since the support structure designs are all the same, the maximum of $F_{i,p}$, $i = 1, 2, 3$ decides the maximum stress on lateral support. $\boldsymbol{F_p}$ denotes the vector composed of these three forces:

$$\boldsymbol{F_p} = \begin{bmatrix} F_{1,p} & F_{2,p} & F_{3,p} \end{bmatrix}. \tag{40}$$

The maximum of these three forces can be expressed as the infinite norm of $\boldsymbol{F_p}$, $\|\boldsymbol{F_p}\|_\infty$. The support structure has to withstand the force $\|\boldsymbol{F_p}\|_\infty$ multiplied by a reasonable safety factor without yielding or buckling.

Compared with the safety of the support structure, the safety of the mirror is much more concerning. The maximum first principal stress on mirror shall not exceed 7 MPa, while the yield strength of the structure is above 200 MPa. However, the stress on the mirror depends not only on the magnitude of the load, but also the direction. As shown in Fig. 8, the stress on the lateral support is caused by shear load F_s and normal load F_p, and the peak stress is on the edge of the lateral support pad.

The normal load F_p causes push/pull stress σ_p, which distributes uniformly on the support area:

$$\sigma_p = F_p / A, \tag{41}$$

where A denotes the bonding area of the support point.

The shear load F_s causes bending stress, which distributes linearly on the area. The peak stress σ_s is on the edge of the support area:

$$\sigma_s = \frac{F_s d L}{2I}, \tag{42}$$

where d is the lateral support pad's thickness, L is the lateral support pad's length, and I is the inertia moment of the lateral support pad's cut section.

Based on calculation, σ_s is much larger than σ_p. σ_s is determined by F_s, and the maximum σ_s on the mirror is determined by maximum shear load $F_{s,p}$. Hence, the maximum shear load $F_{s,p}$ is a more critical requirement. Maximum shear load $F_{s,p}$ can be calculated by F_p and the angle between the shear load with the tangential vector of the mirror edge η:

$$F_{s,p} = \| F_p \cos\eta \|_\infty. \tag{43}$$

The angle η can be calculated by the unit tangential vector $v_{v,i}$ at the support point and the load vector v_i, $i = 1, 2, 3$:

$$v_i = [\cos\alpha_i, \sin\alpha_i], \tag{44}$$

$$v_{t,i} = \frac{[-a^2 y_i, b^2 x_i]}{a^4 y_i^2 + b^4 x_i^2} = \frac{[-a\sin\theta_i, b\cos\theta_i]}{\sqrt{a^2\sin^2\theta_i + b^2\cos^2\theta_i}}, \tag{45}$$

$$\cos\eta_i = \frac{|v_{t,i} v_i|}{|v_{t,i}||v_i|}. \tag{46}$$

The maximum shear load $F_{s,p}$ is also adopted as a metric function Φ_2 that relates to the mirror stress.

B. Dynamic Model for Lateral Support

Resonant frequency is the indicator of system dynamic performance and can be obtained by FEA. M3M's natural resonant frequency is high enough compared with the support system's resonant frequency [12]. So M3M can be treated as a rigid concentric mass with three DOFs in plane and described by a 3×3 mass matrix. The support system can be simplified as springs with equivalent stiffness. In this way, the system is simplified as a planar mechanism, of which dynamic performance can be derived by the Lagrange equation. The system's kinetic energy T and potential energy V are

$$T = \frac{1}{2} M \dot{x}^2 + \frac{1}{2} M \dot{y}^2 + \frac{1}{2} J \dot{\gamma}^2, \tag{47}$$

$$V = \frac{1}{2} K_1 \delta_1^2 + \frac{1}{2} K_2 \delta_2^2 + \frac{1}{2} K_3 \delta_3^2, \tag{48}$$

where M denotes the mirror mass, and J denotes the mirror's moment of inertia. K_1, K_2, and K_3 denote the stiffness of each whiffletree, and they are basically equal since the designs of all the whiffletree components are the same. So they are substituted with a constant K in the following calculation.

Based on the Lagrange equation

$$d/dt(\partial T/\partial \dot{x}_i) - \partial T/\partial x_i = -\partial V/\partial q_i, \tag{49}$$

the dynamic equation can be derived as

$$\begin{bmatrix} M & & \\ & M & \\ & & J \end{bmatrix} \begin{bmatrix} \ddot{x} \\ \ddot{y} \\ \ddot{\gamma} \end{bmatrix} + \begin{bmatrix} k_{11} & k_{12} & k_{13} \\ k_{21} & k_{22} & k_{23} \\ k_{31} & k_{32} & k_{33} \end{bmatrix} \begin{bmatrix} x \\ y \\ \gamma \end{bmatrix} = 0. \tag{50}$$

Both the mass matrix and stiffness matrix are symmetric. The elements of the lower triangle in the stiffness matrix are

$$k_{11} = K\cos^2\alpha_1 + K\cos^2\alpha_2 + K\cos^2\alpha_3, \tag{51}$$

$$k_{21} = K\cos\alpha_1\sin\alpha_1 + K\cos\alpha_2\sin\alpha_2 + K\cos\alpha_3\sin\alpha_3, \tag{52}$$

$$k_{22} = Kd_1\cos\alpha_1 + Kd_2\cos\alpha_2 + Kd_3\cos\alpha_3, \tag{53}$$

$$k_{31} = K\sin^2\alpha_1 + K\sin^2\alpha_2 K_3\sin^2\alpha_3, \tag{54}$$

$$k_{32} = Kd_1\sin\alpha_1 + Kd_2\sin\alpha_2 + Kd_3\sin\alpha_3, \tag{55}$$

$$k_{33} = Kd_1^2 + Kd_2^2 + Kd_3^2. \tag{56}$$

K is evaluated as 2.4×10^4 N/m in the optimization. The specific value of stiffness K has no effect on the optimization result. Solving the equation can get the system's modal frequencies f_1, f_2, and f_3 and the corresponding eigenvector. The first-order resonant frequency f_1 indicates the system's dynamic property.

C. Lateral Support Geometry Optimization

The layout of lateral support geometry needs to balance dynamic and static performances. As mentioned before, the mirror stress is more concerning than the stress on the support structure. Thus, the maximum shear load $F_{s,p}$ is selected as an objective function Φ_1. The first-order resonant frequency of the lateral support system f_1 indicates the dynamic performance. To express the optimization model as a minimum problem, take the opposite number of f_1 as the other objective function:

$$\Phi_1 = F_{s,p}, \tag{57}$$

$$\Phi_2 = -f_1. \tag{58}$$

This is a typical multi-objective optimization problem with two objective functions Φ_1 and Φ_2. The optimization variables are the angle of support points, including θ_1, θ_2, and θ_3, and the angle of support direction, including α_1, α_2, and α_3:

$$\begin{aligned} \min \quad & \Phi_1, \Phi_2 \\ \text{s.t.} \quad & \begin{cases} -\frac{\pi}{4} < \alpha_1 < \frac{\pi}{4} \\ \frac{\pi}{2} < \alpha_2 < \pi \\ -\pi < \alpha_3 < -\frac{\pi}{2} \\ 0 < \theta_1 < \frac{\pi}{2} \\ \frac{\pi}{2} < \theta_2 < \pi \\ \frac{5}{4}\pi < \theta_3 < \frac{7}{4}\pi \\ \|\boldsymbol{F_p}\|_\infty < 0.8\,W \end{cases} . \end{aligned} \tag{59}$$

It is challenging to balance the optimal solutions for all the objective functions. In many cases, there is no absolute optimal solution for multi-objective optimization problems, only Pareto optimal. The neighborhood cultivation genetic algorithm (NCGA) is developed from the genetic algorithm. NCGA can increase the speed of obtaining the Pareto solution set by cross breading the design points of the adjacent Pareto solution set. Therefore, we use NCGA to search for the Pareto solution. Figure 9 plots the figure of the first-order frequency and maximum lateral load of the searched points. The upper design sets have advantages over the lower in terms of dynamic performance. The left design sets have advantages over the right in terms of static performance. The front formed by the points in the upper left is the Pareto optimal. Choosing the points in the Pareto optimal will benefit more than the rest. But there is not an absolute optimized solution in the Pareto optimal. So we choose an optimal design with a moderate performance on both objective functions. Table 2 lists f_1, $\| F_p \|$, $F_{s,p}$ of initial designs and optimal designs. W in the table stands for the gravity load of the mirror, which is about 18 kN. Compared with the initial design, the optimal design increases the first-order modal frequency f_1 by 4.55% and decreases the maximum shear load $F_{s,p}$ by 5.77%.

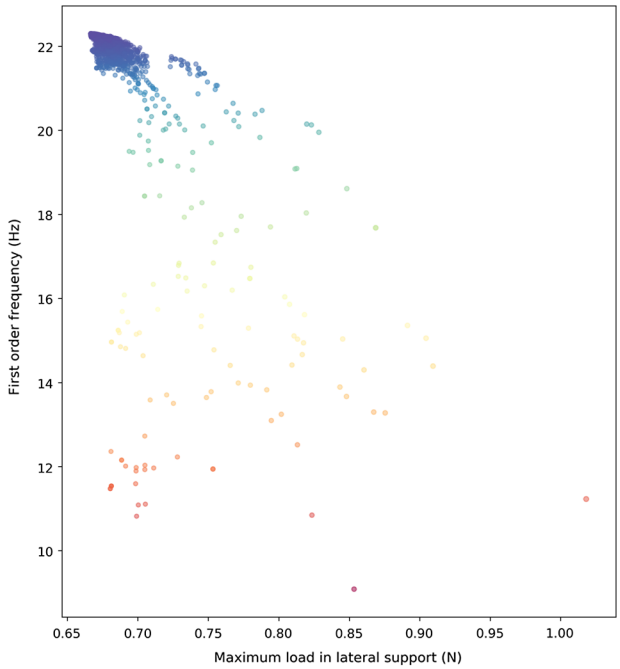

Fig. 9. Explored lateral support design points.

Table 2. Optimization Results of Axial Support

	Initial Design	Optimized Design
α_1(°)	180	170.79
α_2(°)	300	310.55
α_3(°)	60	64.63
θ_1(°)	37.5	45.64
θ_2(°)	140	149.4
θ_3(°)	261	269.85
f_1 (Hz)	17.96	18.78
$\|\boldsymbol{F_p}\|_\infty$	0.7566 W	0.792 W
$F_{s,p}$	0.459 W	0.433 W

6. CONCLUSION

This paper presents some methods to evaluate and optimize the geometric layout of a 3.5 m × 2.5 m thin elliptical mirror.

The axial support efficiency is evaluated by the mirror surface SlopeRMS. By using the adaptive simulated annealing algorithm, the SlopeRMS of the mirror surface under gravity decreases from 1.046 μrad to 1.033 μrad. The mirror surface figure under gravity is not sensitive to lateral support locations. The lateral support geometric layout mainly affects the system's resonant frequency and stress level on the mirror. The first-order resonant frequency f_1 and the maximum reaction F_{max} are optimized by the multi-objective algorithm. For early studies or conceptual designs of opto-mechanical systems, the method in this paper can improve efficiency. With the aid of a simplified model, the job of model building and computing time can be significantly improved.

Funding. National Key Research and Development Program of China (2017YFE0102900); Youth Innovation Promotion Association of the Chinese Academy of Sciences (2016198).

Disclosures. Guo Peng, Jingxu Zhang, Fei Yang, Haifei Hu, Haibo Jiang: Changchun Institute of Optics Fine Mechanics and Physics, FE.

Data Availability. Data underlying the results presented in this paper are not publicly available at this time but may be obtained from the authors upon reasonable request.

REFERENCES

1. P. Schipani, S. D'Orsi, L. Ferragina, D. Fierro, L. Marty, C. Molfese, and F. Perrotta, "Active optics primary mirror support system for the 2.6 m VST telescope," Appl. Opt. **49**, 1234–1241 (2010).
2. D. W. Robinson, "Minimizing gravity sag of a large mirror with an inverted Hindle-mount," Proc. SPIE **4093**, 142–150 (2000).
3. E. Ponslet, V. Stephens, A. Tubb, E. C. Williams, B. Dan, M. Cho, T. Mast, J. Nelson, R. J. Ponchione, and M. Sirota, "Development of the primary mirror segment support assemblies for the Thirty Meter Telescope," Proc. SPIE **6273**, 627319 (2006).
4. H. J. Meier, "Support of thin-meniscus primary for Sofia," Proc. SPIE **1340**, 153–164 (1990).
5. G. Schwesinger, "Lateral support of very large telescope mirrors by edge forces only," J. Mod. Opt. **38**, 1507–1516 (1991).
6. C. Nissly, B. J. Seo, M. Troy, G. Angeli, B. Ellerbroek, L. Gilles, and N. Sigrist, "High-resolution optical modeling of the Thirty Meter Telescope for systematic performance trades," Proc. SPIE **7017**, 70170U (2008).
7. M. K. Cho, "Performance prediction of the TMT tertiary mirror support system," Proc. SPIE **7018**, 70184f (2008).
8. P. Zhou, K. Wang, C. Yan, and X. Zhang, "Research on the degradation of lightweight mirror surface accuracy," Appl. Opt. **57**, 7758–7763 (2018).
9. L. Wei, L. Zhang, X. Gong, and D. Mei Ma, "Design and optimization for main support structure of a large-area off-axis three-mirror space camera," Appl. Opt. **56**, 1094–1100 (2017).
10. Y. Rivenson, T. Liu, Z. Wei, Y. Zhang, K. de Haan, and A. Ozcan, "Phasestain: the digital staining of label-free quantitative phase microscopy images using deep learning," Light Sci. Appl. **8**, 23 (2019).
11. P. Zhou, S. Xu, C. Yan, and X. Zhang, "Research on neutral surface of lightweight, horizontally supported mirror," Opt. Eng. **57**, 025107 (2018).
12. H.-Y. Kihm, H.-S. Yang, I. Kweon Moon, J.-H. Yeon, S.-K. Lee, and Y.-W. Lee, "Adjustable bipod flexures for mounting mirrors in a space telescope," Appl. Opt. **51**, 7776–7783 (2012).